Author(s): Kallunki, Jouni & Alava, Mikko J. & Hellén, E. K. O.

Title: The electric field close to an undulating interface

Year: 2006

Version: Final published version

Please cite the original version:

Kallunki, Jouni & Alava, Mikko J. & Hellén, E. K. O. 2006. The electric field close to an undulating interface. Journal of Applied Physics. Volume 100, Issue 2. 023528/1-6. ISSN 0021-8979 (printed). DOI: 10.1063/1.2211329.

The electric field close to an undulating interface

Jouni Kallunki, Mikko Alava, and E. K. O. Hellén

Citation: Journal of Applied Physics **100**, 023528 (2006); doi: 10.1063/1.2211329
View online: http://dx.doi.org/10.1063/1.2211329
View Table of Contents: http://scitation.aip.org/content/aip/journal/jap/100/2?ver=pdfcov
Published by the AIP Publishing

The electric field close to an undulating interface

Jouni Kallunki and Mikko Alava[a)]
Laboratory of Physics, Helsinki University of Technology, P.O. Box 1100, FIN-02015 HUT Espoo, Finland

E. K. O. Hellén
Oy Keskuslaboratorio-Centrallaboratorium Ab (KCL), P.O.Box 70, FIN-02151 Espoo, Finland

(Received 26 October 2005; accepted 4 May 2006; published online 27 July 2006)

The electric potential close to a boundary between two dielectric material layers reflects the geometry of such an interface. The local variations arise from the combination of material parameters and from the nature of the inhomogeneity. Here, the arising electric field is considered for both a sinusoidally varying boundary and for a "rough," Gaussian test case. We discuss the applicability of a one-dimensional model with the varying layer thickness as a parameter and the generic scaling of the results. As an application we consider the effect of paper roughness on toner transfer in electrophotographic printing. © *2006 American Institute of Physics*.
[DOI: 10.1063/1.2211329]

I. INTRODUCTION

In many applied physics and engineering applications, one is interested in the behavior of static or time-dependent electric field close to a boundary between two dielectric materials. Examples range from semiconductor devices to packaging to paper making, and one may envision in the future nanotechnology applications in which such questions are of importance. The essential mathematical problem at hand is to understand the qualitative and quantitative changes to the homogeneous geometry, where the local field is constant inside both materials. In a typical case (see Sec. II for details), one has a potential difference imposed over a bi- or multilayered sample, such that one or more of the interfaces are undulating or simply nonflat.

The interesting physics and the most pertinent complications ensue, naturally, in the proximity of such an interface and if its "roughness" is of appreciable magnitude. In any case, the practical issues are twofold: developing easy-to-use models for potential applications and understanding the behavior of the electric field variation as a function of parameters that describe the geometry of the boundary layer. For instance, in the case of a sinusoidally varying interface, one has two parameters—the wavelength and amplitude—and the above two issues can be considered in the phase space defined by them. For more general, in particular, disordered or random, boundaries such issues have been studied by using, e.g., perturbation theories for the solution of the static Maxwell equations.[1]

One application area, in which the above-mentioned issues are of importance, is electrophotographic printing.[2] In it colored toner particles are charged and transferred onto the surface of paper using an electric field, which penetrates paper. Elaborate two-dimensional computer simulations with simplified one-dimensional modeling have been used to study the effect of the nonhomogeneous structure of paper on forces acting on toner particles and thus on the transfer efficiency and print quality.[3,4] Our approach here is similar but the viewpoint is somewhat different. We hope that the results below will prove to be useful for various other applications, too. Our main findings concern the validity of the simple one-dimensional solution involving the statistics of interface variation and the scaling of the electric fields in general. As an application we consider in the spirit mentioned above the effect of paper roughness on the electric field in an electrophotographic printing process and compare the results to the existing literature on the field.

The one-dimensional (1D) model, starting with the particular geometry chosen, is derived in Sec. II. In Sec. III we investigate its range of applicability by comparing it to numerical, finite-element-method-based solutions of the problem. Section IV discusses the more general scaling properties of the electric field statistics using artificially created (the so-called Gaussian) interfaces and, again, numerical solutions. In Sec. V we consider electrophotographic printing and show how the model can be used to estimate the local toner transfer efficiency. Finally, in Sec. VI we summarize again our work and finish with a short discussion.

II. A CONTINUUM MODEL

We start by considering a two-dimensional case, illustrated in Fig. 1, where the system consists of three layers. A potential difference is established initially between the bottom side and the top side. The upper and lower interfaces are taken to be flat and at potentials $\phi=0$ and $\phi=V_0$, respectively. The presence of the three layers is of interest here since this case applies to a rough, dielectric plate in contact with a flat layer. The layers are dielectric and we consider a steady state without any electric currents.

The problem is thus to calculate the *static* electric field $\mathbf{E}$ with given boundary conditions at the opposite faces. The system can be described using the standard Gauss law for dielectric media,[5]

[a)]Electronic mail: mja@fyslab.hut.fi

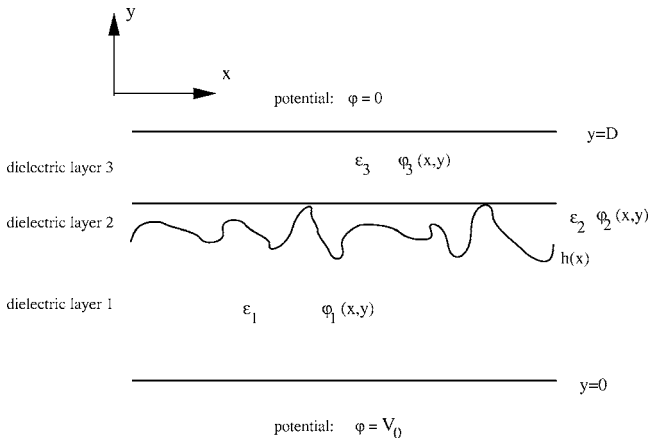

FIG. 1. Illustration of the model geometry and notation.

$$\nabla \cdot [\epsilon_i(x,y)\mathbf{E}_i(x,y)] = -\nabla \cdot [\epsilon_i(x,y)\,\nabla\,\phi(x,y)] = \rho_i(x,y), \tag{1}$$

and the boundary conditions read as

$$\phi_1(x,0) = V_0, \quad \phi_3(x,D) = 0. \tag{2}$$

Here ϵ and ρ denote the permittivity and charge density, respectively, D gives the thickness of the system, and the subindex $i=1,2,3$ is used to refer to different layers. At the interfaces between the layers, the boundary conditions are the common continuity requirements,

$$\begin{aligned}
&\phi_1[x,h(x)] = \phi_2[x,h(x)],\\
&\epsilon_1 \mathbf{n}\cdot\nabla\phi_1[x,h(x)] = \epsilon_2 \mathbf{n}\cdot\nabla\phi_2[x,h(x)],\\
&\phi_2(x,d_1+d_2) = \phi_3(x,d_1+d_2),\\
&\epsilon_2 \mathbf{n}\cdot\nabla\phi_2(x,d_1+d_2) = \epsilon_3 \mathbf{n}\cdot\nabla\phi_3(x,d_1+d_2),
\end{aligned} \tag{3}$$

where $d_1=\langle h(x)\rangle$ is the mean height of the undulating interface and $\mathbf{n}$ denotes the normal vector. This set of equations completely determines the electric potential and the field.

1D approximation

In a complicated geometry, the analytic solution to Eq. (1), fulfilling boundary conditions (2) and (3), is not accessible. Before tackling the problem numerically, it is instructive to analyze the problem by a simple 1D capacitor approximation, illustrated in Fig. 2. Here the spatially varying interface is replaced by its mean value. Another useful or necessary simplification is to replace any local permittivity with an effective value by averaging it over the thickness $\epsilon_i(x,y) \to \epsilon_i(x) = \langle \epsilon_i(x,y)\rangle_y$. A detailed discussion on effective permittivities and the validity of the averaging procedure can be found in Ref. 6; here it will be considered as a parameter which can be measured. Note that the effective permittivity is a *local* average and may still vary spatially.

Now Eq. (1) becomes

$$\frac{\partial^2 \phi(y)}{\partial y^2} = -\frac{\rho_i}{\epsilon_i}, \tag{4}$$

and the boundary conditions reduce to

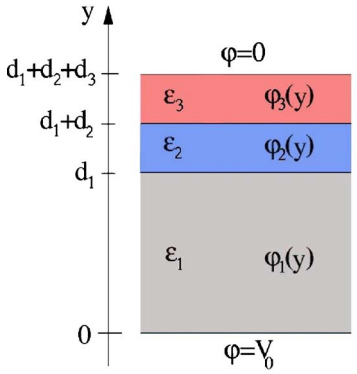

FIG. 2. Illustration of the 1D approximation. The system is locally approximated with a three layer capacitor.

$$\begin{aligned}
&\phi_1(x,0) = V_0, \quad \phi_3(x,d_1+d_2+d_3) = 0,\\
&\phi_1(x,d_1) = \phi_2(x,d_1),\\
&\epsilon_1 \partial_y \phi_1(x,d_1) = \epsilon_2 \partial_y \phi_2(x,d_1),\\
&\phi_2(x,d_1+d_2) = \phi_3(x,d_1+d_2),\\
&\epsilon_2 \partial_y \phi_2(x,d_1+d_2) = \epsilon_3 \partial_y \phi_3(x,d_1+d_2).
\end{aligned} \tag{5}$$

These are easily solved for the potential. We concentrate on the field in the top layer and take $\rho_1=\rho_2=0$ and $\rho_3=\rho$ as this case is considered in the experimental part in Sec. V. The potential takes the form

$$\begin{aligned}
\phi_3(y) &= \frac{-\rho}{2\epsilon_3}[y^2 - (d_1+d_2+d_3)^2]\\
&\quad + \frac{\alpha}{\epsilon_3}(\beta\rho - V_0)(y-d_1-d_2-d_3),\\
\alpha &= \left(\frac{d_1}{\epsilon_1} + \frac{d_2}{\epsilon_2} + \frac{d_3}{\epsilon_3}\right)^{-1},\\
\beta &= \left(\frac{d_1+d_2}{\alpha} + \frac{d_3^2}{2\epsilon_3}\right),
\end{aligned} \tag{6}$$

which leads to the field

$$E_3^{(y)}(y) = -\partial_y \phi_3(y) = \frac{\alpha}{\epsilon_3}\left(V_0 - \frac{\rho d_3^2}{2\epsilon_3}\right) + \frac{\rho}{\epsilon_3}(y-d_1-d_2). \tag{7}$$

Note that all the information of the properties of layers 1 and 2 is included in α.

III. VALIDITY OF 1D APPROXIMATION

The validity of the 1D approximation is studied by comparing the result (7) to the numerical solution of the full two-dimensional (2D) problem. Solving partial differential equations in 2D numerically is a standard problem and many ready made software packages exist for this purpose. We have used the ELMER 3.0 package, developed by the Center for Scientific Computing at Otaniemi, Finland (CSC Ltd),

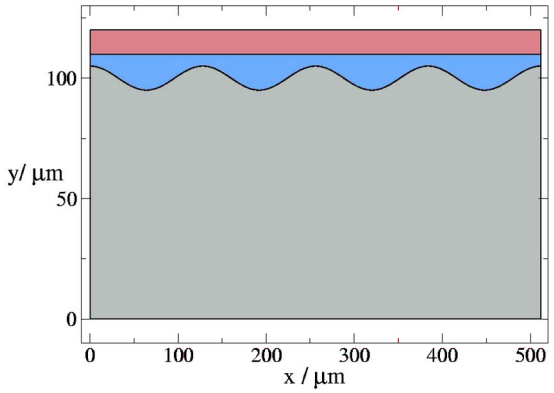

FIG. 3. The system geometry with a perturbed interface. Perturbation amplitude is $H_0=5$ μm and wavelength $\lambda=128$ μm. System size is 120 $\times 512$ μm^2.

which employs the finite-element method. Detailed description on the numerical methodology can be found from the CSC's webpage.[7] The choice of parameters used in the numerical calculations was

$$d_1 = 100\ \mu\text{m}, \quad d_2 = 10\ \mu\text{m}, \quad d_3 = 10\ \mu\text{m},$$
$$\epsilon_1 = 4\epsilon_0, \quad \epsilon_2 = \epsilon_0, \quad \epsilon_3 = 2\epsilon_0, \tag{8}$$
$$\rho_3 = -8.5\frac{C}{m^3},$$

unless stated otherwise. All the numerical results are given in the units of the surface potential of the lowest layer V_0.

The simplest way to quantitatively analyze the 1D approximation is to create sinusoidal surface profiles, with altering wavelengths λ and amplitude H_0: $h(x)=d_1+H_0\sin(2\pi x/\lambda)$. The geometry is illustrated in Fig. 3 and the numerical and 1D results for the field's y component at the middle of the top layer ($y=115$ μm) in Fig. 4. It is clear that the 1D approximation yields a reasonable result for the y component. The x component is about two orders in magnitude smaller, $E^{(x)}/E^{(y)}\approx 0.01$, indicating that the field is to a good approximation in the y direction.

A quantitative criterion for the limit of validity of the 1D approximation can be found by looking at the variation in the field strength A_{num} and comparing it to that of the 1D approximation, A_{1D} (see Fig. 4). The ratio A_{num}/A_{1D} is plotted as a function of the wavelength λ in Fig. 5, for various values of the perturbation amplitude H_0 and bottom layer thickness d_1. The 1D approximation clearly underestimates the effect of long wavelength and overestimates the effect of short wavelength variations. For long wavelengths the situation is not too bad, since the ratio is at most 2.

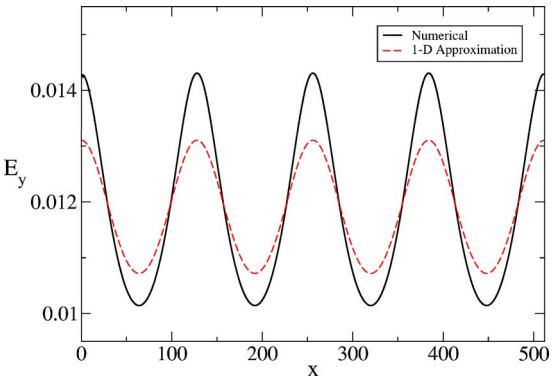

FIG. 4. Comparison of the y component of the electric field between numerical and approximative solutions. Fields are calculated in the middle of the uppermost layer 3 at $y=115$ μm.

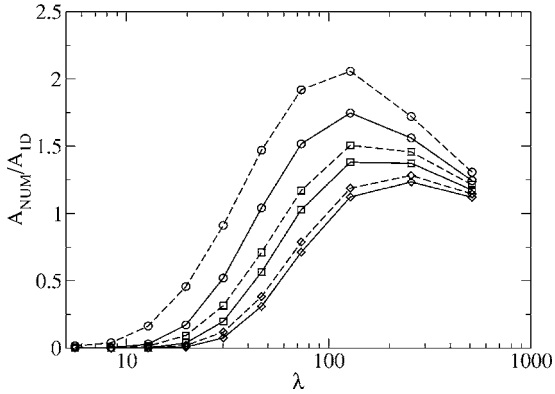

FIG. 5. The ratio of the numerically, A_{num}, and analytically, A_{1D}, determined perturbation amplitudes in the y component for thicknesses $d_1=100$ μm (circle), $d_1=95$ μm (square), and $d_1=90$ μm (diamond) and perturbation amplitudes $H_0=5$ μm (full lines) and $H_0=10$ μm (dashed lines).

The accuracy of the 1D approximation seems to improve as the perturbation is moved further away from the observation point (here it is the middle of the top layer). Intuitively this is clear as the diffusionlike equation (1) tends to smoothen out nonuniformities. The same effect was illustrated in another context in Ref. 3, in which the effect of fillers on the electric field was considered: The deeper the filler particles are located inside the paper, the less they will disturb the field around toner particles.

The fact that the 1D approximation applies further away from the perturbation suggests that the relevant length is the distance between the perturbation and the measurement point, denoted as d_{per}. In Fig. 6 the ratio A_{num}/A_{1D} is replotted but the wavelength is now scaled with d_{per}. The scaling in

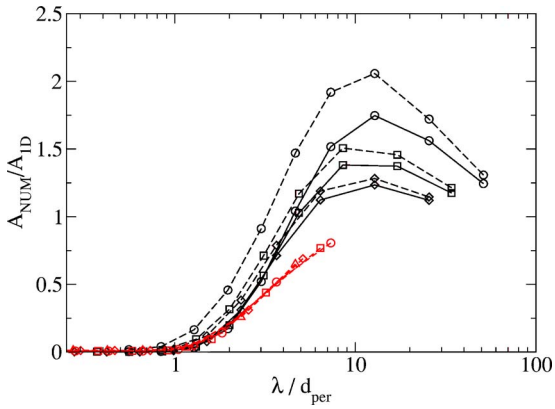

FIG. 6. The ratio of the numerically, A_{num}, and analytically, A_{1D}, determined perturbation amplitudes in the y component for thicknesses $d_1=100$ μm (circle), $d_1=95$ μm (square), and $d_1=90$ μm (diamond) and perturbation amplitudes $H_0=5$ μm (full lines) and $H_0=10$ μm (dashed lines) plotted as a function of the scaled wavelength λ/d_{per}. The red lines are results obtained when the *lower* surface is perturbed instead of the upper side. Notation and parameters are identical to Fig. 5.

wavelength axis is reasonable. It also seems that one could collapse the data further by multiplying the amplitudes by parameter specific values. We leave this aside to demonstrate the actual values of the ratio. Figure 6 shows the ratio also in the case when the perturbation is made for the *lower* surface. In this case the scaling is excellent. Based on this figure it may be estimated that the 1D approximation is applicable for perturbations with a wavelength $\lambda > 3d_{\mathrm{per}}$ and that the perturbations with a wavelength $\lambda < d_{\mathrm{per}}$ are negligible. For the parameters at hand, this means that for the upper (lower) surface $d_{\mathrm{per}} \approx 10$ μm(100 μm), variations on scales below 10 μm(100 μm) are negligible and variations on scales above 30 μm(300 μm) are well described by the 1D approximation.

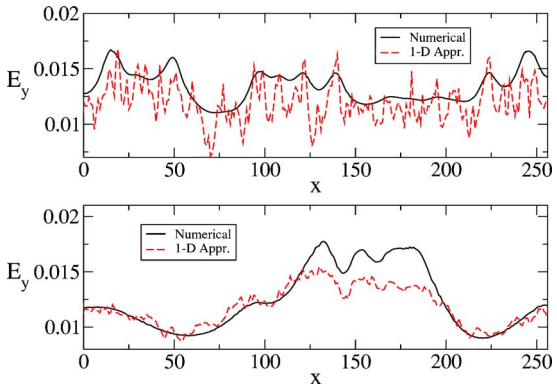

FIG. 7. The y component of the electric field at the middle of the third layer $y=115$ μm obtained for a Gaussian surface of width $\sigma^2=50$ μm^2, with correlation lengths $\xi=2$ μm (upper panel) and $\xi=50$ μm (lower panel).

IV. EFFECT OF SURFACE ROUGHNESS

It is instructive to study how the conclusions made so far apply to a stochastic interface. The simplest possible model for such is the Gaussian interface with exponential correlations

$$P(h) = \frac{1}{\sqrt{2\pi\sigma^2}} \exp\left[-\frac{1}{2\sigma^2}(h-\bar{h})^2 \right],$$
$$\langle h(x) \rangle = \bar{h}, \quad \langle h(x)h(x') \rangle = \sigma^2 \exp\left(\frac{-|x-x'|}{\xi} \right), \tag{9}$$

where σ and ξ are the standard deviation and correlation length, respectively, and $\langle\ \rangle$ denotes an average taken over the relevant distribution. Any variations in the lowest surface enter the model through the *average* thickness $\bar{h}$. Now the layer thicknesses can be written in terms of the height variable h,

$$D = d_1 + d_2 + d_3 = \mathrm{const}, \tag{10}$$

$$d_1 = h, \quad d_2 = D - d_3 - h, \quad d_3 = \mathrm{const}. \tag{11}$$

Gaussian interfaces as above are easily generated numerically. However, if a soft, dielectric medium is brought to contact with a hard one (at the top), the height distribution is modified due to the fact that the medium does not intrude into the top layer. Consequently, the distribution would be cut from above, at a height h_{max} in the simulations. The height distribution then ends to a delta peak with strength $\int_{h_{\mathrm{max}}}^{\infty} dh P(h)$, at h_{max}. A determination of the cutoff height is related to the question of the contact area between the two layers and will not be discussed here.

The numerical result for the field in the top layer and the corresponding 1D approximation are plotted in Fig. 7 for two realizations with correlation lengths $\xi=50$ μm and $\xi=2$ μm. For the $\xi=50$ μm case the analytical approximation works quite well, even though small scale variations present in the 1D result are absent in the full 2D solution. In the other case, $\xi=2$ μm, the small wavelength variations dominate the 1D solution and only the average value of the field is reasonable. This is in line with the results of the previous section, which predict that reliable results are obtained from the 1D approximation for variations at scales $\geqslant 30$ μm, i.e., when $\xi \geqslant 30$ μm.

More precisely this can be seen in the distribution of the y component of the field. The distributions are calculated by averaging the results over an ensemble of 1000 realizations of systems of size 120×512 μm^2. The results for various values of $\xi=2-50$ μm are plotted in Fig. 8. The numerically calculated distributions are compared to the 1D result, which can be calculated analytically[8] with the aid of Eq. (7),

$$P(E_y) = P[h(E_y)] \left| \frac{dE_y}{dh} \right|^{-1}$$
$$= \frac{1}{(E_y - E_0)^2} \frac{1}{\sqrt{2\pi\tilde{\sigma}^2}} \exp\left[\frac{-1}{2\tilde{\sigma}^2} \left(\frac{1}{E_y - E_0} - \mu \right)^2 \right], \tag{12}$$

where

$$E_0 = \frac{\rho}{\epsilon_3}(y - d_1 - d_2), \quad \tilde{\sigma} = \sigma \frac{(\epsilon_3/\epsilon_1) - (\epsilon_3/\epsilon_2)}{V_0 - (\rho/\epsilon_3)(d_3^2/2)},$$
$$\mu = \frac{d_3 + (\epsilon_3/\epsilon_2)(d_1 + d_2)(\epsilon_3/\epsilon_1 - \epsilon_3/\epsilon_2)\bar{h}}{V_0 - (\rho/\epsilon_3)(d_3^2/2)}. \tag{13}$$

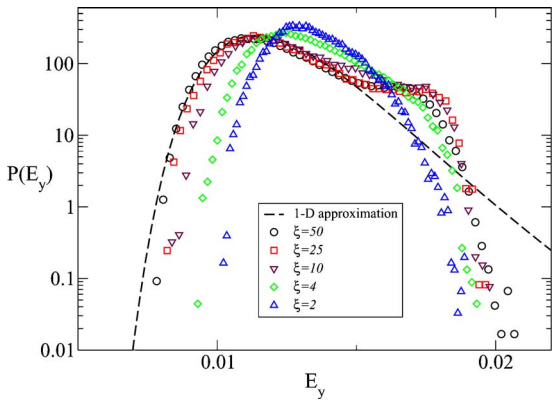

FIG. 8. The distribution of the y component of the field at $y=115$ μm, for various values of ξ ($\sigma^2=50$ μm^2).

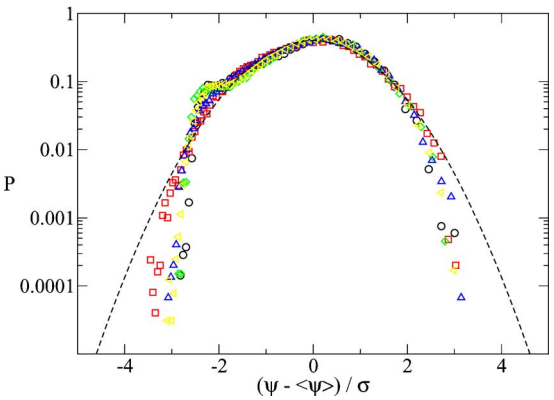

FIG. 9. The scaled distribution of variable ψ. The data before the scaling applied here are the same as in Fig. 8. This is shown at the original $y=115$ μm, for various values of ξ ($\sigma^2=50$ μm^2). Dashed line is the Gaussian distribution with $\sigma^2=1$.

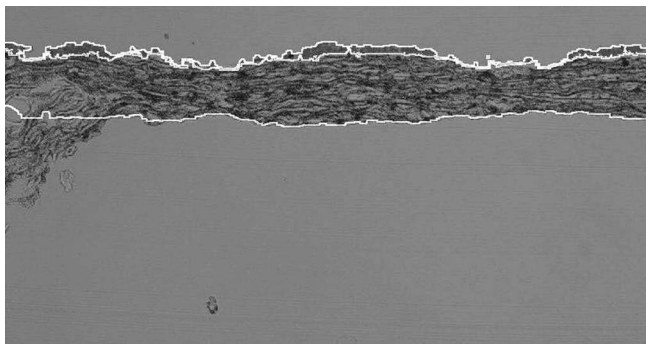

FIG. 10. A cross-section image of a sheet printed with cyan toner at nonoptimal printing conditions. The width of the part of the sheet depicted in the image is 5.3 mm and the interfaces of different layers are denoted by white color. For illustration purposes, the image has been magnified five times more in the vertical direction than in the horizontal one. The average thickness is 120 μm.

From Fig. 8 it is clear that the numerical result agrees very well with the analytical approximation when $\xi \geqslant 30$ μm. For shorter correlation lengths the distribution deviates significantly from the analytical approximation. At high field strengths the analytical distribution should be cutoff, due to the cutoff in the height distribution at $h_{\max}$, and it should end in a delta peak at

$$E_{\max}^{(y)} = \frac{V_0 - (\rho/\epsilon_3)(d_3^2/2)}{d_3 + \epsilon_3 h_{\max}(1/\epsilon_1 + 1/\epsilon_2)} + \frac{\rho}{\epsilon_3}(y - h_{\max}). \quad (14)$$

This peak also appears in the numerical distribution at the right position in a rounded form, after which the distribution dies rapidly.

It turns out that even if the 1D result for the field distribution (12) does not apply directly when the correlation length ξ is short, the *shape* of the distribution remains unaltered. This is easiest to see by defining a new variable

$$\psi = \frac{V_0 - (\rho/\epsilon_3)(d_3^2/2)}{E_3^{(y)} - E_0} = d_3 + \frac{d_1 + d_2}{\epsilon_2} + h\left(\frac{\epsilon_3}{\epsilon_1} - \frac{\epsilon_3}{\epsilon_2}\right). \quad (15)$$

Since ψ depends linearly on the height variable h, the new variable has the same distribution as h, only the mean value is shifted and the width scaled.[9] For the Gaussian interface model the distribution of ψ is then also Gaussian, as seen in Fig. 9. The numerical results are scaled with the numerically determined width σ_{num} and shifted to have a mean value of zero. It is now obvious that the shape of the distribution persists even beyond the validity of the 1D approximation. Thus it may be concluded that the distribution of the y component is given correctly by the 1D result. The two free parameters [a convenient choice is the first two moments of $P(\psi)$] can be determined by the 1D approximation, within its validity, or they have to be determined numerically or, otherwise, experimentally.

V. TONER TRANSFER

The model described above can be directly applied to electrophotographic printing. It is based on transferring charged, colored toner particles from a photoconductor to the surface of paper with an electric field (for an introduction to electrophotographic printing, see, e.g., Ref. 2). Now the lowest layer represents paper with a rough surface to be printed, the topmost layer describes the toner on a photoconductor, which is held at zero potential, and the layer in between is the air gap between paper and toner. During toner transfer, the field gets modified by the structure of paper. This causes variations in the strength of the electrostatic transfer force exerted on toner particles. Large enough variations may lead to undesired variation in the transferred toner amount and to visually observable defects in the print. Both the thickness and local permittivity variations of paper are known to be relevant sources for the field variations.[3,4]

Here we concentrate on the effect of paper roughness on the electric field. A sheet of paper was printed with an electrophotographic printer, where the electric field is created by charging the other side of paper by a corona charger. To emphasize toner transfer nonuniformity, printing conditions were chosen away from optimal, i.e., a too low transfer voltage was used. Print was fixed in an oven after printing to avoid toner movement that would take place in normal hot nip fusing. Figure 10 shows a cross-section micrograph of the printed sheet. The surfaces were extracted from the image and the field was calculated using Eqs. (1)–(3). For simplicity, the toner layer was assumed to be uniform with a constant thickness, permittivity, and charge density, and the permittivity variations of paper were neglected.

Figure 11 compares the electric field strength (calculated in the middle of the toner layer) to the amount of toner transferred. There is a clear correlation between the two even though the toner amount includes shorter wavelength variations than predicted by the model. This is reasonable as there are also other than electric forces involved during the transfer.[9] The close correspondence between the two, illustrated further in the enlarged part displayed in Fig. 12, indicates that in this case the roughness of paper was the dominant source for the variations in the transferred toner amount. In Ref. 3 the effect of thickness (and thus also roughness) variations on print quality was indirectly addressed by comparing the two-point correlation functions of thickness and simulated electric field to each other. Here we have directly demonstrated that there is less toner on locations, where the

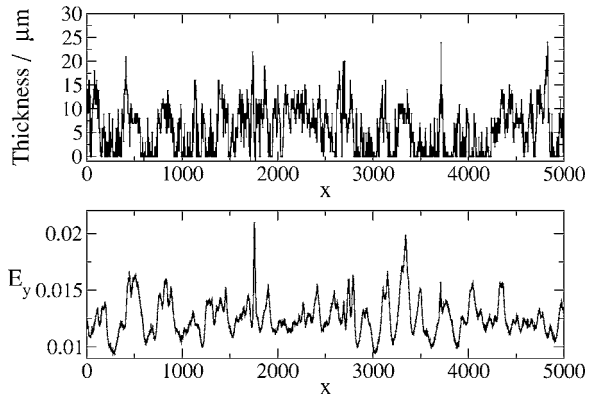

FIG. 11. Comparison between the calculated y component of the electric field (V_0/μm) and the thickness of the transferred toner layer. Vertical scale is in micrometers. Thicknesses used in the computation: $d_1=100$ μm, $d_2=10$ μm, and $d_3=10$ μm.

electric field is low. From the viewpoint of modeling, however, it is important to note that the simple one-dimensional capacitor approximation was accurate enough to capture the essential variations during toner transfer.

VI. SUMMARY AND DISCUSSION

The electric field fluctuations induced by a rough surface are often harmful in practical applications. To obtain quantitative estimates, first one has to be able to measure the "roughness," by direct profilometry or by other means, and then use it to estimate the field variations. One of our goals has been to obtain easy-to-use analytical expressions—the one-dimensional model—which, keeping in mind their range of validity, should prove useful for such purposes.

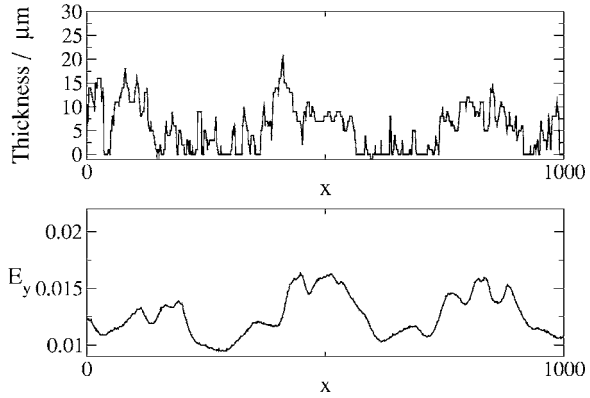

FIG. 12. Comparison between the calculated y component of the electric field (V_0/μm) and the thickness of the transferred toner layer on a magnified scale. Vertical scale is in micrometers. The correlation between the field strength and the transferred toner amount is clear. Thicknesses used in the computation: $d_1=100$ μm, $d_2=10$ μm, and $d_3=10$ μm.

The accuracy of the one-dimensional approximation depends both on the wavelength of the undulating interface and the distance d_{per} to the point at which the field is calculated. The approximation underestimates the effect of long wavelength and overestimates the short wavelength variations. As a rule of thumb, the approximation is reasonably accurate for wavelengths $\lambda > 3d_{\mathrm{per}}$, whereas the wavelengths $\lambda < d_{\mathrm{per}}$ do not significantly contribute to the field. Furthermore, the distribution of field strengths is correctly given by the approximation for all length scales, at least for Gaussian interfaces considered here. For instance, if it is known that a surface has a Gaussian roughness profile, any estimate of its mean-square width would be enough together with the analytical theory.

ACKNOWLEDGMENTS

The Academy of Finland is thanked for its support via the Center of Excellence program (COMP, at HUT) and via an industrial postdoctoral fellowship for one of the authors (J.K.). Pasi Puukko (KCL) is acknowledged for useful discussions.

[1]Some examples are K. W. Yu and T. K. Wan, Comput. Phys. Commun. **142**, 368 (2001); Y. P. Zhao, G.-C. Wang, T.-M. Lu, G. Palasantzas, and J. Th. M. De Hosson, Phys. Rev. B **60**, 9157 (1999).
[2]D. M. Pai and B. E. Springett, Rev. Mod. Phys. **65**, 163 (1993).
[3]A. Cassidy, M. Grant, and N. Provatas, Modell. Simul. Mater. Sci. Eng. **12**, 91 (2004).
[4]N. Provatas, A. Cassidy, and M. Inoue, *Proceedings of IS&T's NIP20: International Conference on Digital Printing Technologies, Salt Lake City UT, 31 October–November 2004* (The Society for Imaging Science and Technology, Springfield, VA, 2004), p. 958.
[5]J. Vanderlinde, *Classical Electromagnetic Theory* (Wiley, Singapore, 1993).
[6]A. Sihvola and J. Kong, IEEE Trans. Geosci. Remote Sens. **26**, 420 (1988).
[7]See CSC webpage, http://www.csc.fi/elmer/index.phtml, for more information.
[8]N. G. van Kampen, *Stochastic Processes in Physics and Chemistry* (North-Holland, Amsterdam, 1981).
[9]D. S. Rimai, D. S. Weiss, and D. J. Quesnel, J. Adhes. Sci. Technol. **17**, 917 (2003).